# SPIN–ORBIT COUPLING IN BIRADICALS. 3. HEAVY ATOM EFFECTS IN CARBENES*

Zdenek HAVLAS[a] and Josef MICHL[b]

[a] *Institute of Organic Chemistry and Biochemistry, Academy of Sciences of the Czech Republic, 166 10 Prague 6, Czech Republic; e-mail: havlas@uochb.cas.cz*

[b] *Department of Chemistry and Biochemistry, University of Colorado, Boulder, CO 80309-0215, U.S.A.; e-mail: michl@eefus.colorado.edu*

Received June 25, 1998
Accepted June 29, 1998

*Dedicated to Professor Rudolf Zahradnik on the occasion of his 70th birthday.*

CASSCF(8,6)/cc-pVDZ calculations of electron spin–spin dipole interaction tensor in the lowest triplet state of $CH_2$, CHF, CHCl, and CHBr, spin–orbit coupling of each of the three sublevels with the lowest singlet, and the triplet zero-field-splitting parameters are reported as a function of the valence angle, with bond lengths optimized for the triplet state at the B3LYP/cc-pVTZ level of approximation. Both the one- and the two-electron parts of the spin–orbit coupling Hamiltonian are used, and the contributions to spin–orbit coupling provided by each atom and orbital pair in Weinhold's natural hybrid orbital basis are evaluated separately. This provides intuitive insight into the origin of spin–orbit coupling in carbenes and especially, the heavy atom effect of the substituent.

**Key words:** Carbenes; Spin–orbit coupling; Spin–spin dipolar coupling; Zero-field-splitting parameters; *Ab initio* calculations.

Triplet biradicals occur as intermediates in many organic photochemical reactions and their conversion to final products normally involves intersystem crossing from the lowest triplet state $T_1$ into the lowest singlet state $S_0$. One of the factors that dominate the absolute rate of this step, and relative rates at various geometries, is the strength of spin–orbit coupling. Its dependence on molecular structure and conformation has been the subject of many calculations[1] and can be understood in intuitive terms, which involve the formulation of resonance structures that contain triplet carbene or twisted ethylene substructures[2]. A simple rationalization of spin–orbit coupling in carbene and its derivatives is therefore desirable. The situation in $CH_2$ itself has been analyzed in detail recently and numerous references to prior work were provided[3].

* Part 2: see ref.[3]

In addition to influencing the rate of intersystem crossing, spin–orbit coupling is also capable of affecting the triplet zero-field-splitting parameters, used in EPR spectroscopy to describe the relative energies of the three triplet sublevels. We refer to the values calculated in the usual approximation, which neglects spin–orbit coupling contributions, as $D$ and $E$, and to the full values that can actually be observed, as $D'$ and $E'$.

Presently, we address the issue of the heavy atom substituent effect in halocarbenes, *i.e.*, the enhancement of intersystem crossing rate and changes in the triplet zero-field-splitting parameters due to the presence of atoms with high atomic numbers. Some of the preliminary results have been reported[4] and several of these values are now updated with an improved computational procedure.

Monohalogenated carbenes have been the subject of numerous experimental and theoretical studies. High-resolution spectroscopy[5–8] proved that they have a singlet ground state. The $S_0$–$T_1$ singlet–triplet energy difference decreases as the atomic number of the halogen increases, from 14.9 kcal/mol in CHF (refs[9,10]), and 4.2 kcal/mol in CHCl (ref.[9]) to a mere 2.6 kcal/mol (ref.[9]) in CHBr (ref.[8]). *Ab initio* calculations[11,12] yielded the values of 16 kcal/mol (CHF), 6 kcal/mol (CHCl), and 4 kcal/mol (CHBr). To the best of our knowledge, no observations or calculations of the triplet zero-field-splitting and spin–orbit coupling in these molecules have been published. The importance of spin–orbit coupling for the interpretation of spectra of CHCl and CHBr was emphasized by Chang and Sears[7,8].

## METHOD OF CALCULATION

The method of calculation has been described in detail[1]. Only the procedure for the evaluation of the two-electron parts in atomic contributions and in contributions of individual natural hybrid orbital[13] pairs to spin–orbit coupling has been slightly modified. Inspection of the individual terms showed that the two-electron elements of the type[3] $h^{(2)}_{\mu\nu\rho\sigma}$ contribute significantly only if two of the subscripts are equal. Terms in which all four subscripts are different give less then 1% of the total two-electron contribution in all calculations presented in this paper. In the most important among the $h^{(2)}_{\mu\nu\rho\sigma}$ terms, $\rho$ represents an inner shell orbital. An electron in such an orbital screens the nucleus on which the orbital is centered, and the sign of $h^{(2)}_{\mu\nu\rho\sigma}$ is opposite to that of the one-electron term $h^{(1)}_{\mu\nu}$. Therefore, in the definition of orbital pair contributions, the $h^{(2)}_{\mu\nu\rho\sigma}$ element is counted as contributing to the $\mu,\nu$ orbital pair, and to the atomic vector of the nucleus on which $\rho$ is located.

The calculations were performed with CASSCF(8,6) wave functions using the cc-pVDZ basis set[14] on all atoms except Br, for which the pVDZ basis set[15] was used. Orbitals in the triplet and singlet CASSCF wave functions were optimized separately, with the constraint of common core orbitals taken from the triplet calculation. The non-bonding orbitals $A$ and $B$ are the open-shell orbitals of the $T_1$ wave function. In the

analysis of the results, pre-orthogonal natural hybrid orbitals (NHOs) of the $T_1$ state were used as the most appropriate.

## RESULTS AND DISCUSSION

Figure 1 shows the calculated potential energy curves of carbene and the halocarbenes as a function of the HCX valence angle ω at bond lengths optimized for the lowest triplet state $T_1$ at each value of ω. As anticipated from prior work[10], fluorine is the most strongly interacting substituent and in CHF the lowest singlet state $S_0$ lies significantly below $T_1$ even at geometries optimized for the latter. The singlet-stabilizing effect of the halogen drops as its atomic number increases.

### *Spin–Spin Dipolar Coupling*

The electron spin–spin dipolar tensor of carbene in its $T_1$ state is not affected much by the presence of the halogen atom. Figure 2 compares the values of the spin-only zero-field-splitting parameters *D* and *E* calculated by tensor diagonalization, ignoring any corrections for spin–orbit coupling. Halogen substitution does not significantly affect the small gradual diminution of *D* induced by decrease of the valence angle from a linear (ω = 180°) geometry. The substitution reduces the *D* values somewhat, undoubtedly because it permits some of the spin density to delocalize onto the halogen, thus increasing the average distance between the unpaired electrons (Table I). The substitution also makes the *E* value somewhat more negative, particularly in CHF. This accentuation of the anisotropy between the *x* and *y* directions can be attributed to preferential spin delocalization by π as opposed to σ delocalization.

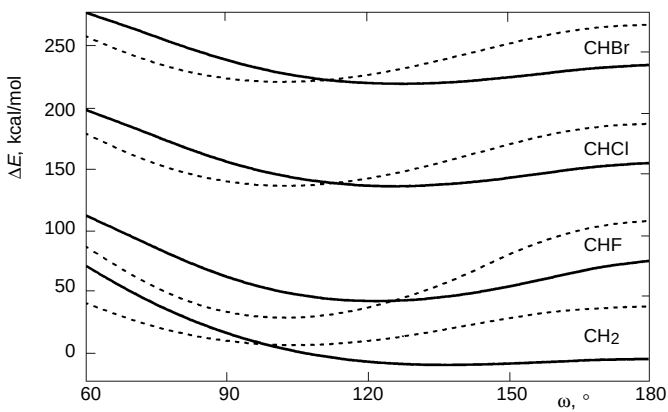


FIG. 1

Potential energy of carbenes at triplet-optimized geometries (B3LYP/cc-pVTZ) relative to $T_1$ energy at 180°, as a function of the valence angle ω. Solid line: $T_1$, dashed line: $S_0$. Curves for successive carbenes shifted up by 80 kcal/mol

The orientation of the principal directions *y* and *z* of the spin–spin dipolar coupling tensor in the CHX molecular frame for a series of valence angles HCX is shown in Fig. 3 (the *x* direction is perpendicular to the molecular plane), and is very much the same as it was in $CH_2$ itself, in keeping with the discussion above. The labeling of the *x*, *y*, and *z* axes follows the usual EPR convention[16], which makes $T_z$ the lowest-energy and $T_x$ the highest-energy triplet sublevel in this instance. In the case of $CH_2$ this differs from the usual symmetry convention in that it uses the label *y* for the twofold symmetry axis.

*Spin–Orbit Coupling*

Symmetry allows only two of the three sublevels of the $T_1$ state to mix with the lowest singlet state. The $S_0$–$T_1$ spin–orbit coupling vector $\boldsymbol{H}^{SO}$ thus has only two non-zero components, $\langle S | H^{SO} | T_y \rangle y$ and $\langle S | H^{SO} | T_z \rangle z$, and lies in the molecular plane *yz*. Figure 4 shows its length $H^{SO} = (\langle S | H^{SO} | T_y \rangle^2 + \langle S | H^{SO} | T_z \rangle)^{1/2}$ as a function of the valence angle ω. The huge heavy atom effect is clearly apparent. The shape of the dependence is the same for all of the carbenes: $H^{SO}$ is nearly independent of ω until quite large angles are reached, and then it drops abruptly and reaches zero at 180° by symmetry. In terms of the simple model of Part 1 (ref.[2]), which describes the wave functions of the $S_0$ and $T_1$ states as mixtures of the singlet configuration functions *AB*, $A^2 - B^2$, and $A^2 + B^2$, where *A* and *B* are the "non-bonding" orbitals of the carbene, the rationalization is simple: $H^{SO}$ vanishes at 180° since it is proportional to the coefficient of the symmetrized hole-pair configuration $A^2 + B^2$ in the wave function of $S_0$. At the linear geometry the contribution of $A^2 + B^2$ to $S_0$ vanishes, because CHX then is a perfect axial biradical, with a degenerate $S_0$, $S_1$ state described by the wave functions $A^2 - B^2$ and *AB*, and without any contribution from $A^2 + B^2$.

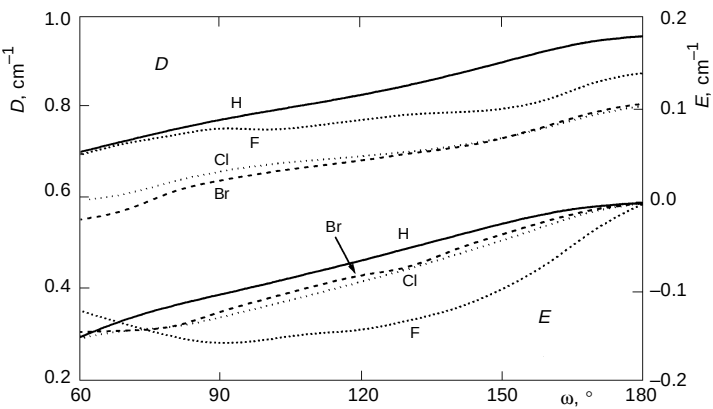


FIG. 2

Spin–spin dipolar contributions *D* and *E* to zero-field-splitting parameters in carbenes as a function of the valence angle ω

In $CH_2$ itself, symmetry constrains the vector $\mathbf{H}^{SO}$ to lie along the *z* axis, and for the particular choice of state wave function phases that we made, it points in its positive direction. In halocarbenes, $\boldsymbol{H}^{SO}$ is not constrained by symmetry, but at most geometries it still lies approximately along *z* (Figs 3 and 4). We have chosen analogous wave function phases in all cases, and $\boldsymbol{H}^{SO}$ always points up.

*Atomic Contributions to the Spin–Orbit Coupling Vector*

Figure 3 indicates the vectorial contributions of the individual atoms to the total spin–orbit coupling vector $\boldsymbol{H}^{SO}$ for selected HCX valence angles ω. The contributions of the hydrogen atoms are entirely negligible, and in $CH_2$, the only significant contribution to

TABLE I
Non-bonding orbitals *A* and *B* of carbenes in the basis of pre-orthogonal NHOs $A_i$ and $B_j$, as a function of the CHX valence angle ω[a]

| CHX | ω, ° | $A_1$ | $A_2$ | $B_1$ | $B_2$ | $B_3$ | $B_4$ | $B_5$ |
|---|---|---|---|---|---|---|---|---|
| $CH_2$ | 60 | 0.98 | – | –0.91 | –0.12 | –0.12 | – | – |
| | 90 | 0.98 | – | –0.92 | –0.14 | –0.14 | – | – |
| | 120 | 0.98 | – | –0.95 | –0.11 | –0.11 | – | – |
| | 150 | 0.98 | – | –0.97 | –0.09 | –0.09 | – | – |
| | 180 | 0.99 | – | –0.99 | 0.0 | 0.0 | – | – |
| CHF | 60 | 0.98 | –0.34 | –0.59 | –0.14 | –0.17 | 0.13 | 0.45 |
| | 90 | 0.99 | –0.42 | –0.88 | –0.29 | –0.25 | 0.17 | 0.39 |
| | 120 | 0.99 | –0.43 | –0.89 | –0.30 | –0.29 | 0.20 | 0.36 |
| | 150 | 1.00 | –0.43 | –0.88 | –0.24 | –0.25 | 0.17 | 0.33 |
| | 180 | 1.00 | –0.42 | –1.00 | 0.0 | 0.0 | 0.0 | 0.42 |
| CHCl | 60 | 0.96 | –0.39 | –0.57 | –0.12 | –0.50 | 0.12 | 0.48 |
| | 90 | 0.96 | –0.50 | –0.83 | –0.25 | –0.21 | 0.24 | 0.40 |
| | 120 | 0.97 | –0.52 | –0.88 | –0.23 | –0.21 | 0.28 | 0.37 |
| | 150 | 0.98 | –0.51 | –0.94 | –0.21 | –0.19 | 0.23 | 0.40 |
| | 180 | 1.00 | –0.46 | –1.00 | 0.0 | 0.0 | 0.0 | 0.46 |
| CHBr | 60 | 0.95 | –0.40 | –0.56 | –0.17 | –0.47 | 0.11 | 0.48 |
| | 90 | 0.94 | –0.50 | –0.81 | –0.23 | –0.21 | 0.26 | 0.39 |
| | 120 | 0.95 | –0.51 | –0.86 | –0.21 | –0.20 | 0.29 | 0.36 |
| | 150 | 0.97 | –0.48 | –0.92 | –0.18 | –0.17 | 0.24 | 0.38 |
| | 180 | 0.99 | –0.43 | –0.99 | 0.0 | 0.0 | 0.0 | 0.43 |

[a] Expansion coefficients of $A_1$ and $A_2$ in molecular orbital *A* and of $B_1$–$B_5$ in molecular orbital *B*.

$\boldsymbol{H}^{SO}$ is provided by the carbon atom. As one goes to the halocarbenes, the carbon contribution changes somewhat, but it gradually becomes totally insignificant relative to the much larger contribution provided by the halogen atom as the atomic number of the latter increases (note the change of scale on the right in Fig. 3). The direction of the vectorial contribution due to the halogen atom is approximately parallel to that of the carbon contribution, and even in CHF, where the contribution of the fluorine atom is only about twice that of the carbon atom, there is no doubt that the vector sum will be longer than either atomic contribution alone, making spin–orbit coupling stronger. This corresponds to the ordinary heavy atom substituent effect. In CHCl, and even more so, in CHBr, the carbon contribution is essentially negligible, and its direction is immaterial. Still, the HCX valence angle ω is decisive for the orientation of the contribution that the halogen atom makes to $\boldsymbol{H}^{SO}$. As ω increases, the contribution of the halogen atom, and thus the whole resultant $\boldsymbol{H}^{SO}$ vector as well, gradually rotate to the left side of the C–Hal bond when viewed from the carbon.

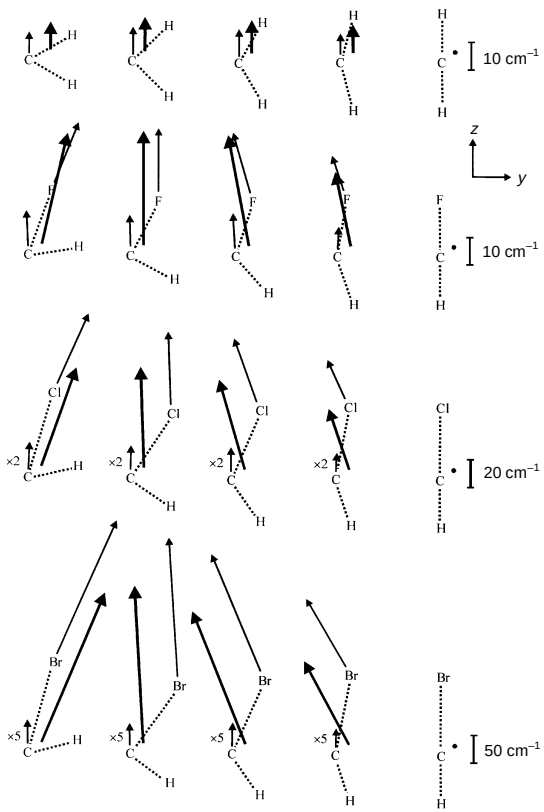


FIG. 3
Orientation of carbene framework in the magnetic axes *y* and *z* , spin–orbit coupling vectors $\boldsymbol{H}^{SO}$ (thick arrows), and atomic vectorial contributions to $\boldsymbol{H}^{SO}$ (thin arrows)

The key to understanding this behavior is provided by the data given in Table II, which lists the contributions to the total spin–orbit coupling vector from the individual natural hybrid orbital (NHO) pairs displayed in Fig. 5a. In each pair, the first member makes a contribution to the π-symmetry carbene non-bonding orbital *A*, which is empty in the simple description of the $S_0$ state. The other makes a contribution to the σ-symmetry carbene non-bonding orbital *B*, doubly occupied in the simple description of $S_0$.

At all valence angles, there are only two important contributors to *A*, labeled $A_1$ and $A_2$ in Fig. 5a, both of π symmetry. Orbital $A_1$ is the p orbital on carbon and orbital $A_2$ is the p orbital on the halogen that normally carries one of the three lone pairs of the halogen substituent and acts as a π donor. Since *A* is the higher energy molecular orbital of the two that result from the interaction of the atomic orbitals $A_1$ and $A_2$, it represents their out-of-phase combination, as indicated by shading in Fig. 5a.

TABLE II

Contributions of NHO pairs $A_i$–$B_j$ to the spin–orbit coupling vector length $\boldsymbol{H}^{SO}$ in carbenes, as a function of the CHX valence angle ω[a]

| CHX | ω, ° | Pairs $A_1$–$B_j$ | | | Pairs $A_2$–$B_j$ | |
|---|---|---|---|---|---|---|
| | | $B_1$ | $B_2$ | $B_3$ | $B_4$ | $B_5$ |
| $CH_2$ | 60 | 11.0 (0) | 4.7 (–108) | 4.7 (108) | – | – |
| | 90 | 11.6 (0) | 2.5 (–112) | 2.5 (112) | – | – |
| | 120 | 11.8 (0) | 2.1 (–108) | 2.1 (108) | – | – |
| | 150 | 9.7 (0) | 1.3 (–101) | 1.3 (101) | – | – |
| CHF | 60 | 9.2 (–7) | 2.0 (90) | 1.9 (–17) | 4.8 (–104) | 24.9 (–12) |
| | 90 | 13.7 (14) | 4.2 (–97) | 3.8 (121) | 11.6 (55) | 21.7 (–30) |
| | 120 | 15.2 (7) | 4.1 (–97) | 4.2 (118) | 12.4 (71) | 22.0 (–17) |
| | 150 | 11.3 (3) | 1.9 (–99) | 2.1 (108) | 7.1 (84) | 17.1 (–8) |
| CHCl | 60 | 5.5 (–2) | 1.0 (90) | 2.0 (46) | 10.6 (–107) | 63.8 (–15) |
| | 90 | 8.9 (4) | 2.7 (–90) | 2.3 (119) | 40.6 (50) | 51.1 (–35) |
| | 120 | 9.4 (4) | 2.3 (–98) | 2.1 (113) | 41.4 (65) | 50.7 (–23) |
| | 150 | 8.2 (2) | 1.2 (–90) | 1.0 (107) | 24.5 (81) | 44.3 (–10) |
| CHBr | 60 | 5.0 (–5) | 1.0 (90) | 2.6 (53) | 56.1 (–106) | 271.0 (–14) |
| | 90 | 8.1 (4) | 2.5 (–90) | 2.0 (109) | 187.1 (47) | 203.7 (–38) |
| | 120 | 8.6 (0) | 2.1 (–90) | 1.8 (107) | 190.7 (64) | 195.6 (–24) |
| | 150 | 7.6 (2) | 1.1 (–90) | 1.0 (105) | 119.1 (81) | 168.0 (–10) |

[a] In $cm^{-1}$. In parentheses, angle φ (°) at which the spin–orbit coupling vector $\boldsymbol{H}^{SO}$ is directed relative to the positive direction of the *z* axis (measured counterclockwise, *cf.* Figs 3, 4, and 5a).

The σ-symmetry non-bonding molecular orbital *B* is more complicated. Its primary constituent is the σ-symmetry lone pair NHO on carbon, $B_1$. The other two σ-symmetry NHOs on the carbon atom, $B_2$ and $B_3$, are only minor contributors. However, interactions with σ orbitals on the halogen delocalize *B* from its primary site on carbon onto the halogen atom. This is mostly due to a quite significant anti-periplanar interaction of the carbon NHO $B_1$ with a halogen in-plane p NHO $B_5$, ordinarily carrying a second lone pair of the halogen substituent (the third lone pair of the halogen is mostly s in character and is lower in energy). This interaction involves an in-plane overlap that is

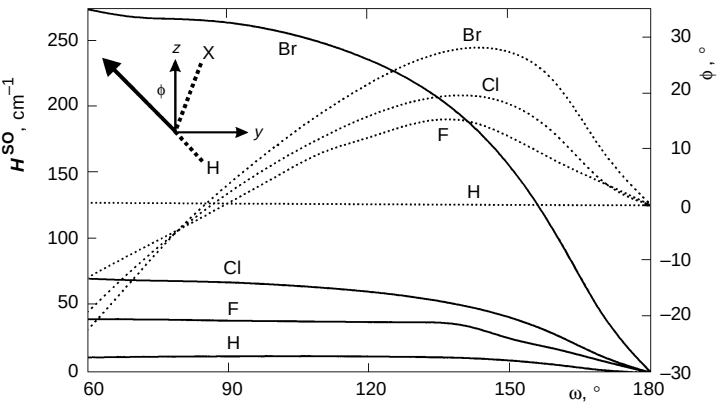


FIG. 4

Carbenes: length of the spin–orbit coupling vector $\boldsymbol{H}^{SO}$ (solid line) and its angle φ with the *z* axis (dashed line) as a function of the valence angle ω

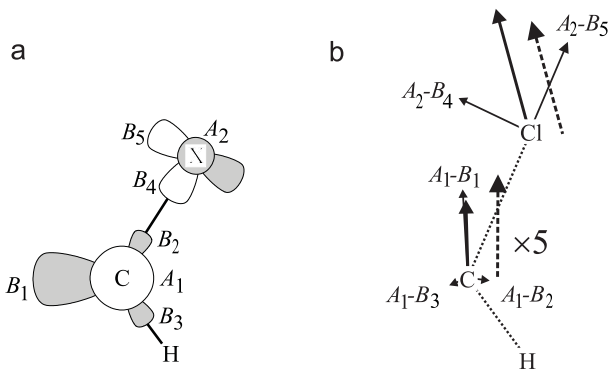


FIG. 5

a Pre-orthogonal NHOs in carbenes (shading indicates their signs in non-bonding molecular orbitals *A* and *B*). b Contributions to $\boldsymbol{H}^{SO}$ in CHCl (ω = 120°): NHO pair contributions (thin arrows), their sums on C and on Cl (thick arrows), and total atomic contributions (dashed arrows). The NHO pair and total atomic contributions on C are scaled by a factor of 5

mostly π in character, and is responsible for σ delocalization. At some angles, this σ interaction mixes in equally strongly also the halogen atom NHO $B_4$ that is used to make the CX σ bond. Once again, since the non-bonding molecular orbital *B* is the least stable of the orbitals that result from the σ mixing, it is not surprising that the NHOs $B_1$ and $B_5$ enter *B* in a mutually antibonding fashion. The coefficients of the constituent NHOs $A_1$ and $A_2$ in the molecular orbital *A*, and of the NHOs $B_1$, $B_4$, and $B_5$ in the molecular orbital *B*, are collected in Table I (the coefficients on $B_2$ and $B_3$ are small and less interesting).

An atomic vectorial contribution to $\boldsymbol{H}^{\mathbf{SO}}$ normally is a resultant of several contributions, each due to a pair of NHOs, one contributing to the molecular orbital *A*, the other to *B*. The most important among these are one-center terms, due to a pair of NHOs centered on the atom. The contribution to $\boldsymbol{H}^{\mathbf{SO}}$ provided by a pair of NHOs with partial p character located on an atom is particularly easy to evaluate when each NHO contributes to only one of the non-bonding orbitals *A* and *B*, and not to the other[3]. This situation is encountered in the carbenes CHX, where *A* is of π and *B* of σ symmetry.

The direction of the vectorial contribution from a pair of NHOs located on the same center is perpendicular to the two axes of their p components. To determine its sense, the NHOs are represented by their p orbital constituents drawn with their signs as they appear in orbitals *A* and *B* (Fig. 5a). The p orbital that is contained in orbital *B* is then rotated into positive overlap with the p orbital contained in orbital *A*. When the direction of this rotation is indicated with the curved fingers of the left hand, its thumb points in the direction of the vectorial contribution to $\boldsymbol{H}^{\mathbf{SO}}$. The directions of all contributions from NHO pairs would reverse their sign if one changed the order of the orbitals *A* and *B*, or if one multiplied one of the orbitals by –1, but this would not affect the relative disposition of the contributions. Since only the absolute values of the components of the spin–orbit coupling vector $\boldsymbol{H}^{\mathbf{SO}}$ are observable, and not its sense, this does not affect the arguments as long as they are made consistently.

Thus, as the p component of the NHO $B_1$ at the carbon atom in Fig. 5a is rotated with the shaded side away from and light side towards the reader, into positive overlap with the p component of the NHO $A_1$, a vectorial contribution to $\boldsymbol{H}^{\mathbf{SO}}$ pointing up on the page, approximately along the positive *z* direction, is generated. On the halogen atom, $A_2$ is out of phase with $A_1$, and $B_5$ is out of phase with $B_1$, so the sense of the rotation required for estimating the $A_2 - B_5$ contribution remains the same and the contributed vector will therefore again point up, approximately along the C–X bond. The vectorial contributions from the major players on the carbon and the halogen atoms will therefore be approximately parallel and mutually reinforcing. Clearly, this is due to the fact that both in the molecular orbital *A* and in the molecular orbital *B*, the two important NHOs of the substituent atom, $A_2$ and $B_5$, are separated by the same number of nodes from the critical orbitals at the carbon atom, $A_1$ and $B_1$, namely one. If one wished to find an example of an inverse heavy atom effect, in which the vectorial contributions

from the carbon and the substituent would be opposed and the length of the vector sum would have an opportunity to be smaller than it was on carbon alone before a heavy-atom substituent was introduced, one would need to break this phase relation. Thus, if the contributions from $B_1$ and $B_5$ were out of phase in the molecular orbital *B*, as in Fig. 5a, but the contributions from $A_1$ and $A_2$ were in phase in the molecular orbital *A*, the vectorial contributions from the $A_1$–$B_1$ and the $A_2$–$B_5$ pairs would be approximately opposed. We are currently examining molecular structures that are likely to meet this requirement.

The situation in halocarbenes is complicated by the fact that the substituent NHO $B_4$ also mixes into the σ-symmetry non-bonding molecular orbital *B*, to a degree that is sensitive to the HCX valence angle ω (Table I). The contribution due to the $A_2$–$B_4$ pair will be pointed in a direction approximately perpendicular to the C–X bond. Since in most cases $B_4$ enters with the sign shown in Fig. 5a, the contribution due to the $A_2$–$B_4$ pair will usually point left and will deflect the total contribution of the halogen atom to the left of the carbon-to-halogen bond vector. This happens especially clearly in the middle range of valence angles around 120°. An illustration is provided in Fig. 5b, which shows how closely the $A_2$–$B_5$ contribution points along the C–X bond, and the $A_2$–$B_4$ contribution perpendicular to the bond. It also illustrates how close the sum of the two leading pair interactions on the halogen, and the one leading interaction on carbon, come to being equal to the total atomic contributions on these atoms.

It is noteworthy that rather small admixtures of the $A_2$ orbital into the molecular orbital *A* and, particularly, of the $B_4$ and $B_5$ orbitals into the molecular orbital *B* (Table I), suffice to dominate the total $\boldsymbol{H}^{\mathrm{SO}}$ vector. Clearly, the magnification provided by the high atomic number nucleus turns spin–orbit coupling into an exquisite probe of molecular orbital delocalization.

*One- and Two-Electron Contributions to Spin–Orbit Coupling*

An important issue for possible future simplification in the calculation of spin–orbit coupling in much larger molecules has to do with the use of an effective one-electron spin–orbit coupling operator. This has seen much use in the past without rigorous testing on polyatomic molecules, but our results support it so far. Thus, in all of the calculations reported here, the ratio of the 2-electron to the 1-electron portions in the contributions from individual orbital pairs, as well as contributions from individual atoms, is remarkably constant. On carbon, it is $-44 \pm 8\%$, on fluorine, $-30 \pm 1\%$, on chlorine, –(17–18%), and on bromine, –(9–10%), independent of the compound and the valence angle. It remains to be seen how general this is across a wider spectrum of molecules.

*Zero-Field-Splitting Parameters*

Finally, in addition to examining the effect of heavy atom substitution on spin–orbit coupling and the likely intersystem crossing rates, we inspect its effect on the zero-field-splitting parameters. The values $D$ and $E$ obtained without spin–orbit coupling (Fig. 2) did not differ much from those of carbene itself. When spin–orbit coupling between the $T_1$ and $S_0$ levels is introduced to obtain the actually observable values $D'$ and $E'$, the situation changes dramatically (Fig. 6).

As in carbene itself[1], the $T_x$ and $T_y$ level energies are not affected much, since the spin–orbit vector is mostly directed along $z$. As a result, the $E$ and $E'$ values are nearly the same. In contrast, the $T_z$ level is shifted strongly, particularly in the region where the $T_1$ and $S_0$ levels attempt to cross. At geometries for which $T_1$ lies below $S_0$, $S_0$–$T_1$ interaction pushes $T_z$ farther below the average of $T_x$ and $T_y$ and $D'$ becomes larger than $D$. At geometries for which $T_1$ lies above $S_0$, $T_z$ is shifted in the opposite direction and $D'$ becomes smaller than $D$. As discussed in more detail elsewhere[3], near the exact point of $T_1$–$S_0$ crossing the usual three-level analysis of the triplet EPR spectrum is not valid and the $D$ and $E$ parameters are ill defined. This is reflected in Fig. 6 as a divergence.

Given the strong dependence of the computed $D'$ values on the valence angle, and thus on vibrational averaging, the uncertainties in the exact location of the $T_1$–$S_0$ crossing point, and the limited accuracy of our calculations, we do not believe that we can

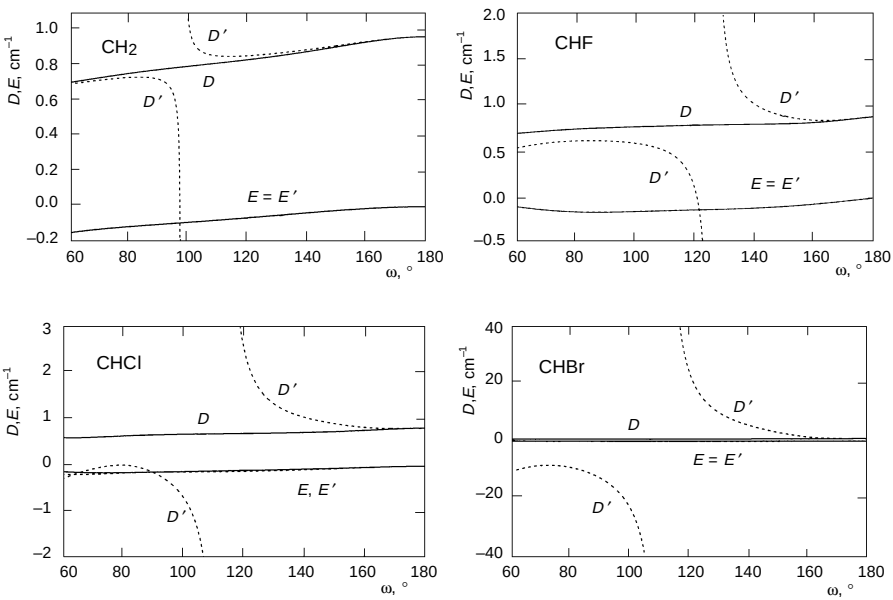


FIG. 6
Zero-field-splitting parameters in carbenes as a function of the valence angle ω. Spin–spin dipolar part ($D$, $E$) and sum of spin–spin dipolar and spin–orbit parts ($D$, $E'$)

make reliable numerical predictions of the zero-field parameters for halocarbenes, although we think that the trends apparent in Fig. 6 are predicted correctly.

## CONCLUSIONS

The present results for halocarbenes can be summarized as follows: (i) The presence of the halogen atom has little effect on the spin–spin dipolar interaction tensor of carbene. (ii) In halocarbenes, the spin–orbit coupling vector $\boldsymbol{H}^{SO}$ is directed in the molecular frame roughly as in carbene itself. (iii) The magnitude of $\boldsymbol{H}^{SO}$ grows dramatically as the atomic number of the halogen increases, and depends on the HCX valence angle ω similarly as in carbene itself, for reasons that are readily understood in terms of the simple model of Part 1 (ref.[2]). (iv) The atomic vectorial contributions of the halogen atoms to $\boldsymbol{H}^{SO}$ are pointed roughly in the same direction as the contribution of the carbon atom. They overshadow the latter even in CHF, and more so in the heavier analogues. (v) Analysis of the results in terms of NHO pair contributions[2] provides detailed understanding and illustrates how a small degree of delocalization of the nonbonding orbitals dominates the overall results for $\boldsymbol{H}^{SO}$. (vi) The ratio of one-electron and two-electron contributions to the atomic and orbital pair contributions to $\boldsymbol{H}^{SO}$ is very constant for each type of atom, boding well for simplified methods in which only the one-electron part is considered explicitely. (vii) In $CH_2$ and CHF, the zero-field-splitting parameters $D'$ and $E'$ are dominated by the spin–spin dipolar coupling contributions $D$ and $E$ except at valence angles located in the vicinity of the $S_0$–$T_1$ crossing point. In CHCl and CHBr, this is still true for the $E'$ values, but the $D'$ values are dominated totally by spin–orbit effects and are very large.

*This work was supported by the NSF (grants CHE-9318469, CHE-9709195, and CHE-9412767).*

## REFERENCES

1. Klessinger M. in: *Theoretical Organic Chemistry; Theoretical and Computational Chemistry* (C. Parkanyi, Ed.), Vol. 5, p. 581. Elsevier, Amsterdam 1998.
2. Michl J.: *J. Am. Chem. Soc*. **1996**, *118*, 3568.
3. Havlas Z., Downing J. W., Michl J.: *J. Phys. Chem. A* **1998**, *102*, 5681.
4. Michl J., Havlas Z.: *Pure Appl. Chem*. **1997**, *69*, 785.
5. Kakimoto M., Saito S., Hirota E.: *J. Mol. Spectrosc*. **1981**, *88*, 300.
6. Suzuki T., Saito S., Hirota E.: *J. Mol. Spectrosc*. **1981**, *90*, 447.
7. Chang B.-C., Sears T. J.: *J. Chem. Phys*. **1995**, *102*, 6347.
8. Chang B.-C., Sears T. J.: *J. Chem. Phys*. **1996**, *105*, 2135.
9. Gilles M. K., Ervin K. M., Ho J., Lineberger W. C.: *J. Phys. Chem*. **1992**, *96*, 1130.
10. Brahms D. L. S., Dailey W. P.: *Chem. Rev*. **1969**, *96*, 1585.
11. Irikura K. K., Goddard W. A. III, Beauchamp J. L.: *J. Am. Chem. Soc*. **1992**, *114*, 48.
12. Shimizu H., Gordon M. S.: *Organometallics* **1994**, *13*, 186.

13. a) Reed A. E., Weinstock R. B., Weinhold F.: *J. Chem. Phys*. **1985**, *83*, 735; b) Reed A. E., Curtiss L. A., Weinhold F.: *Chem. Rev*. **1988**, *88*, 899.
14. a) Dunning T. H., Jr.: *J. Chem. Phys*. **1989**, *90*, 1007; b) Kendall R. A., Dunning T. H., Jr., Harrison R. J.: *J. Chem. Phys*. **1992**, *96*, 6796; c) Woon D. E., Dunning T. H., Jr.: *J. Chem. Phys*. **1993**, *98*, 1358.
15. Schafer A., Horn H., Ahlrichs R.: *J. Chem. Phys*. **1992**, *97*, 2571.
16. Weltner W., Jr.: *Magnetic Atoms and Molecules*, Chap. 3. Van Nostrand Rheinhold, New York 1983.